Supporting Information

Slow DNA Transport through Nanopores in Hafnium Oxide Membranes

*Joseph Larkin,[†¥] Robert Henley,[†¥] David C. Bell,[‡] Tzahi Cohen-Karni,[#] Jacob K. Rosenstein,[§] and Meni Wanunu[†]**

[†]Departments of Physics and Chemistry/Chemical Biology, Northeastern University, Boston, MA 02115; [‡]School of Engineering and Applied Sciences, Harvard University, Cambridge, MA 02138; [#]David H. Koch Institute for Integrative Cancer Research, Massachusetts Institute of Technology, Cambridge, MA 02139; [§]School of Engineering, Brown University, Providence, RI 02912, United States.

TABLE OF CONTENTS:

S1. HfO_2 deposition characterization……2

S2. Elemental analysis of freestanding HfO2 membranes……3

S3. HfO_2 e-beam induced membrane crystallization……4

S4. Dependence of pore conductance on diameter and thickness……5

S5. Determination of peak dwell time……6

S6. Comparison of dsDNA translocation in SiN_x and HfO_2 pores……7

S7. Sequence of the 89 nucleotide molecule……8

S8. α-hemolysin (α-HL) measurements of single-stranded DNA……8

S9. Determination of capture rate for ssDNA……9

S10. Continuous current traces……9

References ……14

Supporting Information

S1. HfO_2 deposition characterization

Thickness of HfO_2 films was calibrated using ellipsometry to determine the mean thickness of HfO_2 per ALD cycle. We have assumed a literature refractive index of $n = 2.0$ for our measurements, which agreed with our measured trajectories for Δ and Ψ. Sixteen ALD cycles of HfO_2 were deposited on a bare <111> silicon wafer, and the thickness of the resulting layer was measured with ellipsometry in several spots on the wafer. This process was repeated several times on the same wafer. HfO_2 thickness was found to increase linearly with the number of ALD cycles. Figure S1a shows this measured HfO_2 thickness after various numbers of ALD cycles, yielding a mean deposition rate of 1.4 Å/cycle.

Surface roughness of deposited HfO_2 surfaces was determined using an AFM. AFM scans of the HfO_2-coated Si wafers described above were performed after each series of ALD cycles. Figure S1b displays the relationship between number of ALD cycles and measured RMS or average surface roughness.

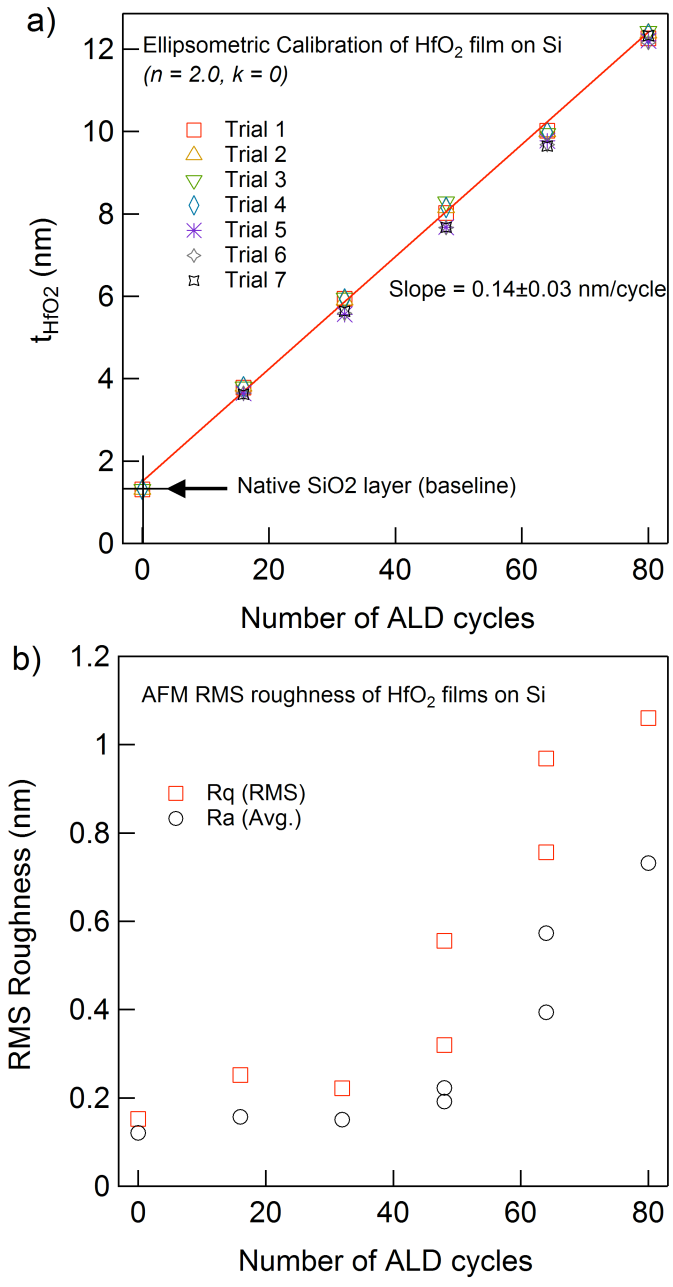

Figure S1. Thickness and roughness characterization of ALD HfO_2. a) Thickness measurements of HfO_2 deposited on a <111> Si wafer in 7 different areas indicate a linear growth of HfO_2 with number of ALD cycles, with an average of 0.14 nm/cycle. b) AFM scans demonstrate increasing surface roughness of HfO_2 with number of ALD cycles.

S2. Elemental analysis of freestanding HfO2 membranes. Energy dispersive x-ray spectroscopy (EDS) maps of different elements were obtained at Harvard University's Center for Nanoscale Systems with a Zeiss Libra 120 TEM at 80 kV equipped with and EDAX Genesis EDS system. For each elemental map, the peak signals from K- and L-series X-rays were added up at each pixel. Figure S2a shows the clear hafnium signal from the ALD-deposited membrane, with silicon, nitrogen, oxygen, and fluorine (present from SF_6 etching) peaks identified in S2b. In Figure S2c, we show the results of elemental maps of Si and N. These are EDS scans where the signals from the peaks identified in 2b have been added up at each pixel. In the dark square, where the SiN_x has been etched, we see the Si and N signal drop to the noise level, as expected from fabrication. The Hf and O scans contains little information (see 2c), as HfO_2 is present at the same thickness throughout the whole image.

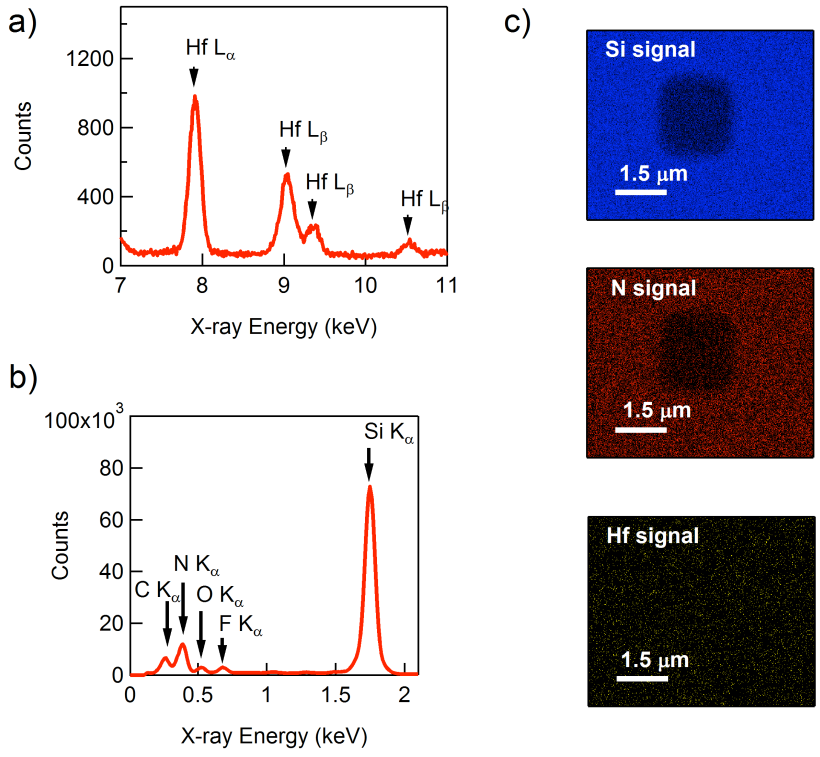

Figure S2. EDS characterization of the HfO_2 membrane. a) EDS spectrum of various hafnium lines taken from the free-standing HfO_2 region of the membrane indicating presence of hafnium. b) EDS spectra showing carbon, nitrogen, oxygen, fluorine, and silicon also present in the film. c) EDS elemental map from an area of membrane that has been etched down to free-standing HfO_2. The brightness of each pixel represents the signal from the corresponding peak in b). We clearly see silicon and nitrogen removed in square region where we etch. As expected, the hafnium signal is uniform, as it was deposited uniformly over the whole area.

S3. HfO_2 e-beam induced membrane crystallization

When the HfO_2 membrane is exposed to a slightly condensed electron beam in the JEOL 2010FEG transmission electron microscope (TEM), it slowly changes from an amorphous HfO_2 layer to a polycrystalline one. This process occurs at an electron dose of 10^6 e/nm^2, which is not enough to drill a pore.[1] The HfO_2 membrane in the TEM image in Figure S3a has been exposed to the partially condensed beam. The central area shows crystalline atomic arrangement and the surrounding membrane exhibits greater thickness variation than the rest of the HfO_2 layer. This variation is evidenced by the changing contrast around the crystallized region, which correspond to sample thickness variations in a TEM image. Figure S3c illustrates this crystallization by showing reduced FFT's of the amorphous and crystalline regions. The region that has been exposed to the condensed beam exhibits peaks in its FFT characteristic of crystallization, while the amorphous region, which has not experienced condensed electron beam irradiation, has an FFT with no clear structure. Figure S3b shows this area after a pore has been drilled with the fully condensed electron beam. The pore may be made fully crystalline, but after piranha cleaning, the crystalline sections of the membrane are completely removed, perhaps due to a strain mismatch between it and the surrounding amorphous material.

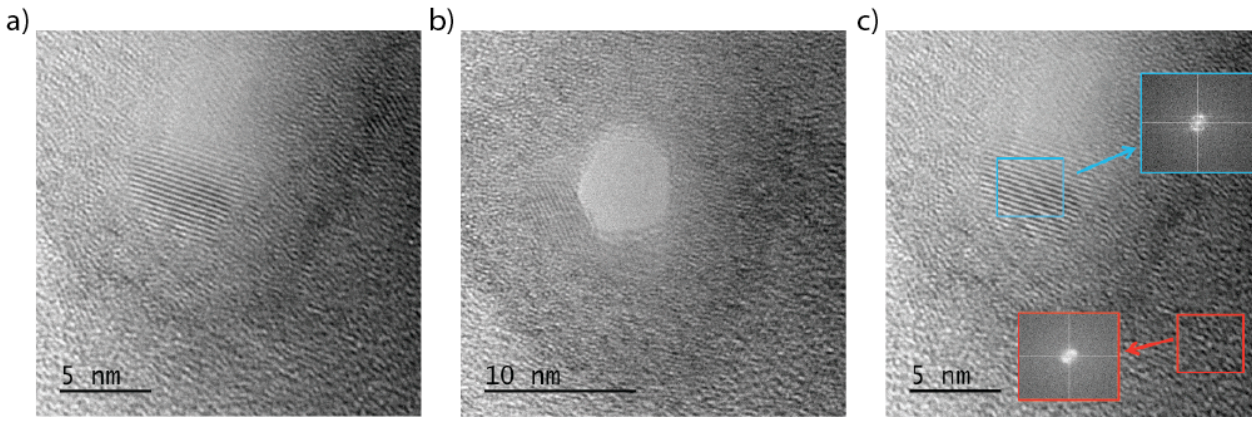

Figure S3. Demonstration of crystallization of the HfO_2 membrane. a) After irradiation with a 200 kV electron beam, a region of the HfO_2 membrane crystallizes. Additionally, the area surrounding the crystallized region shows thickness variations demonstrated in this image by changing contrast. b) A pore drilled in the crystallized area shows sharp lines around the edges from the local crystallinity of the HfO_2. c) FFTs of the identified square regions show crystallinity (bright dots in FFT) in the crystal region and an unstructured FFT in the amorphous region.

S4. Dependence of pore conductance on diameter and thickness

We determine the diameter and thickness of the pore using a geometrical model of conductance, as described in the main text.[2, 3] In the Figure S4, we plot the measured conductance of pores of several different diameters. On the same axes, we plot the conductance curves from the geometrical model for three different pore heights. The height of h = 4.5 nm agrees best across all pores, with one 2 nm pore and some as thick as 7 nm. However, based on the ALD calibration presented in S1, we expect that each pore is in the thickness range of 2 – 3 nm. As discussed in S3, the drilling process crystallizes membrane in the area of the pore, and generally causes local membrane thickness variation. We attribute the pores' unexpectedly high thicknesses to an increase in membrane height due to this e-beam induced change in HfO_2 structure. It seems that pores drilled in the smallest amount of time possible show the least increase in membrane thickness.

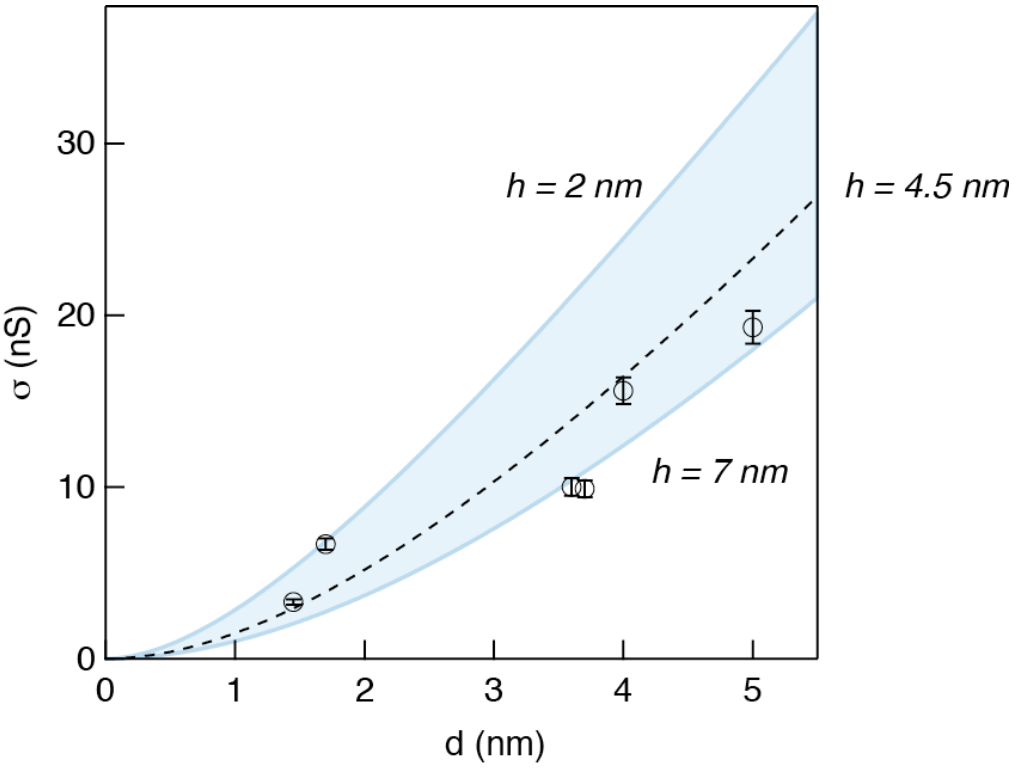

Figure S4. Dependence of pore conductance on pore diameter. Spots indicate measured conductance for HfO_2 pores of different diameters. The lines plot the expected conductance curves using the model presented in the paper with three different pore heights, h = 2 nm, h = 4.5 nm, and h = 7 nm. We expect, based on ALD calibration, that the heights will be 2 – 3 nm, but crystallization during drilling tends to increase film thickness.

S5. Determination of peak dwell time

To determine the peak dwell time, $\langle t_d \rangle$, we first plot a histogram of the logarithm of every t_d in a given data set. For the double-stranded DNA (dsDNA) data, this histogram is normally distributed. We perform a least squares fit of the histogram to a Gaussian. The position of this Gaussian's mean is quoted as $\langle t_d \rangle$, and represents the characteristic dwell time for the experiment. This analysis is illustrated in Figure S5a for the dsDNA data at 250 mV. For single stranded DNA (ssDNA) experiments, the log histogram has two peaks—one representing collision events and the other translocations. We then fit the data to two Gaussians. The position of the mean for the longer dwell time peak is quoted as $\langle t_d \rangle$. The width of the corresponding Gaussian is the spread given in Figure 5d in the main text. This analysis process is illustrated in Figure S5b for data from the 1.4 nm pore at 500 mV.

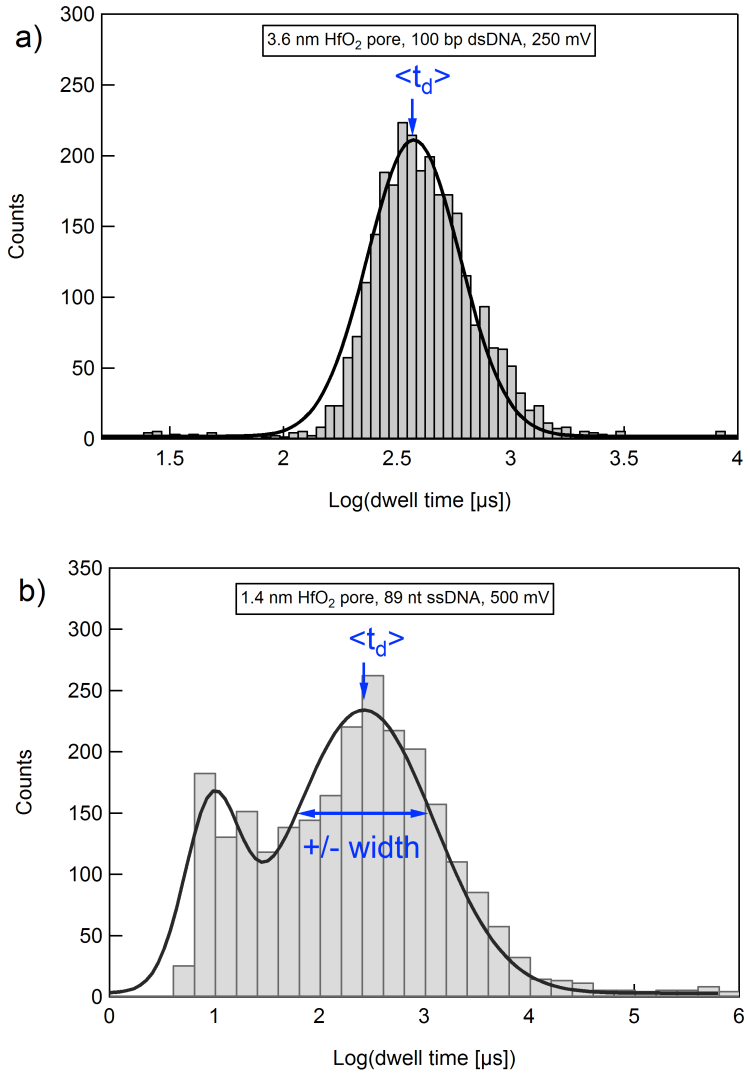

Figure S5. Dwell time analysis. a) The histogram of dwell times for a dsDNA experiment fits to a single Gaussian. The mean position is quoted as $\langle t_d \rangle$. b) For ssDNA, the dwell times fit to two Gaussians, with the longer-time peak representing translocations.

S6. Comparison of dsDNA translocation in SiN_x and HfO_2 pores

In Figure S6, we present a comparison of the 3.6 nm HfO_2 pore studied in this paper to a SiN_x pore of similar diameter and comparable effective thickness from a previous study (h_{eff} = 7 nm for HfO_2 and 10 nm for SiN_x).[4] We compare the interactions between dsDNA molecules and these pores by examining molecular velocity in the pores. The y-axis in Figure S6 represents the average velocity of a molecule in the pore obtained by dividing the length of the sample dsDNA polymer by the mean dwell time. If the translocation process were simply electrophoretic, we would expect a linear dependence of this velocity on applied voltage. However, we see an exponential dependence for both pores. This shows that there is an energetic barrier to the translocation process. The origin of this barrier is the interaction between the DNA molecules and the walls of the pore.[4] By comparing the rate constants from each exponential fit, we see a stronger exponential dependence for the HfO_2 pore than for the SiN_x pore. We point out that the HfO_2 slope is larger despite the fact that the SiN_x pore is slightly thicker, which in principle should yield more interactions that result in a larger dependence on voltage. Thus, we interpret this finding as evidence that the HfO_2 pore walls interact more strongly with dsDNA than those of the SiN_x pore.

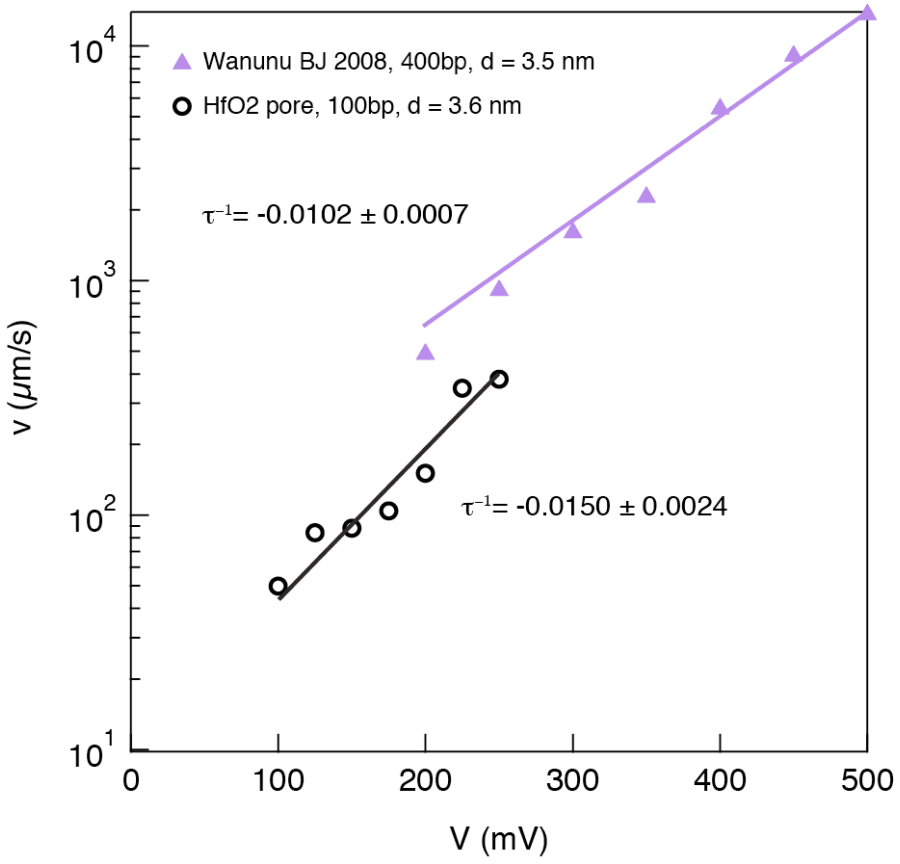

Figure S6. Comparison of dsDNA/pore interaction in HfO_2 and SiN_x pores. Exponential dependence of average molecular velocity on applied voltage is evidence of strong interaction between the molecule and the pore walls. The steeper exponential dependence for HfO_2 (h_{eff} = 7nm) than for SiN_x (h_{eff} = 10 nm) indicates stronger interaction with dsDNA.

S7. Sequence of the 89 nucleotide molecule

The 89 nucleotide molecule was purchased from Stanford Protein and Nucleic Acid Facility. Its sequence is CTCACCTATCCTTCCACTCATACTATCATTATCTACATCTACCATTCATTCAGATCTCACT ATCGCATTCTCATGCAGGTCGTAGCCXZ in the 5' → 3' direction. X is an abasic residue and Z is a 3 spacer C3 CPG modification.

S8. α-hemolysin (α-HL) measurements of single-stranded DNA

To compare the HfO_2 nanopores in our study to α-HL, we performed translocation experiments with the same 89-nucleotide molecule used in this paper through a lipid-embedded α-HL channel (n ~ 300). In Figure S7, we plot the fractional blockades ($\Delta I/I_O$) for an experiment carried out at V = 120 mV. We interpret the peak near $\Delta I/I_O \approx 0.4$ as collision events and the peak at $\Delta I/I_O \approx 0.8$ as translocations. The fractional blockage for the 1.4 nm HfO_2 pore in our study is 0.83, which is quite close to that of the α-HL. While the HfO_2 experiments were carried out at higher voltage, we take this as a practical comparison for current blockage level.

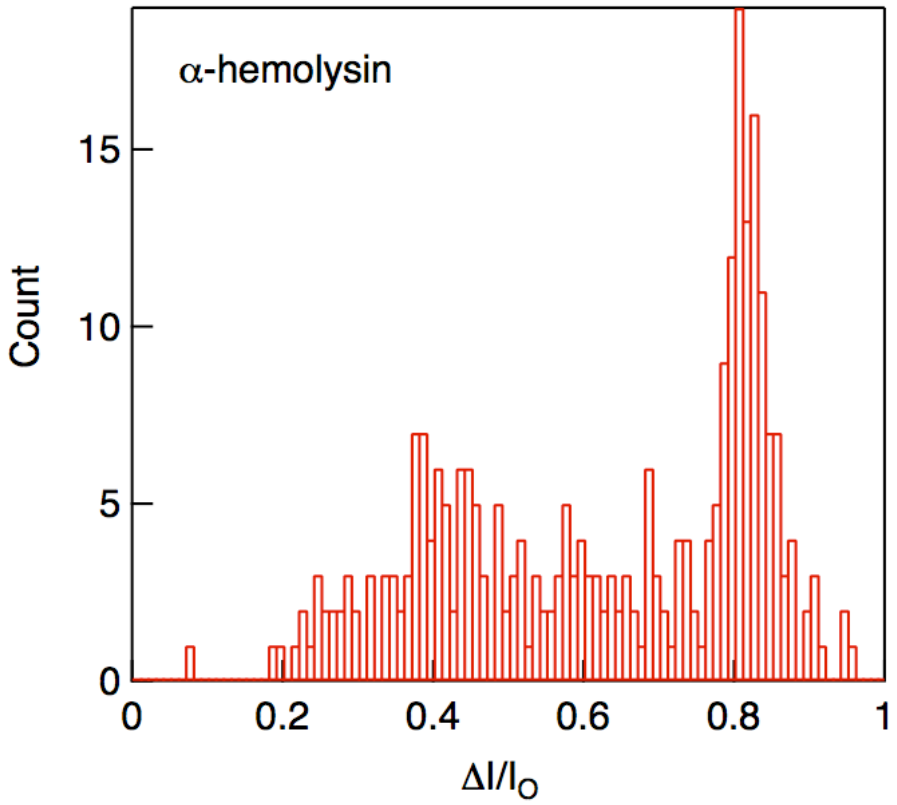

Figure S7. Translocations of the 89 nucleotide molecule in α-hemolysin. The fractional blockage of the HfO_2 nanopores in this study is quite close to that of α-hemolysin.

S9. Determination of capture rate for ssDNA

As with dsDNA, we expect the capture of ssDNA into our pore to be Poissonian, and for the distribution of inter-event times to be exponential.[5] We then perform a least squares fit of our δt histograms to an exponential. In Figure S8, we show these histograms and their fits at each experimental voltage. The inverse time constant of each exponential fit is the capture rate at the given voltage.

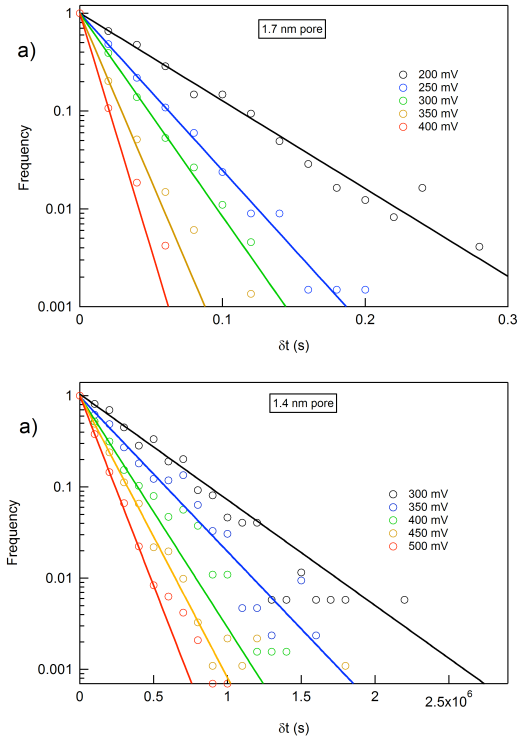

Figure S8. ssDNA capture rate analysis. a) The histograms of inter-event times for ssDNA in a 1.7 nm HfO_2 pore with exponential fits. b) The histograms of inter-event times for ssDNA in a 1.4 nm HfO_2 pore with exponential fits.

S10. Continuous current traces

In Figures S9-S12, we present several raw, continuous time traces for HfO_2 pores. S9 displays 10 seconds of highly uniform translocation data of 100 bp DNA through the 3.6 nm HfO_2 pore at three different voltages. S10 and S11 show similar traces for the 89 nucleotide molecules in, respectively, the 1.7 and 1.4 nm pores. Figure S12 shows 50 seconds of data for the 1.4 nm pore at three different

voltages. At several points, we see the current drop and then rise sharply. This is due to an automated pore-clearing routine, which applies a large negative voltage pulse when the pore's conductivity has fallen below a certain threshold for a predetermined period of time. The ensuing current decay back to the open pore level is indicative of the membrane's capacitance. These prolonged dips in conductivity may occur when a molecule becomes stuck in the pore.

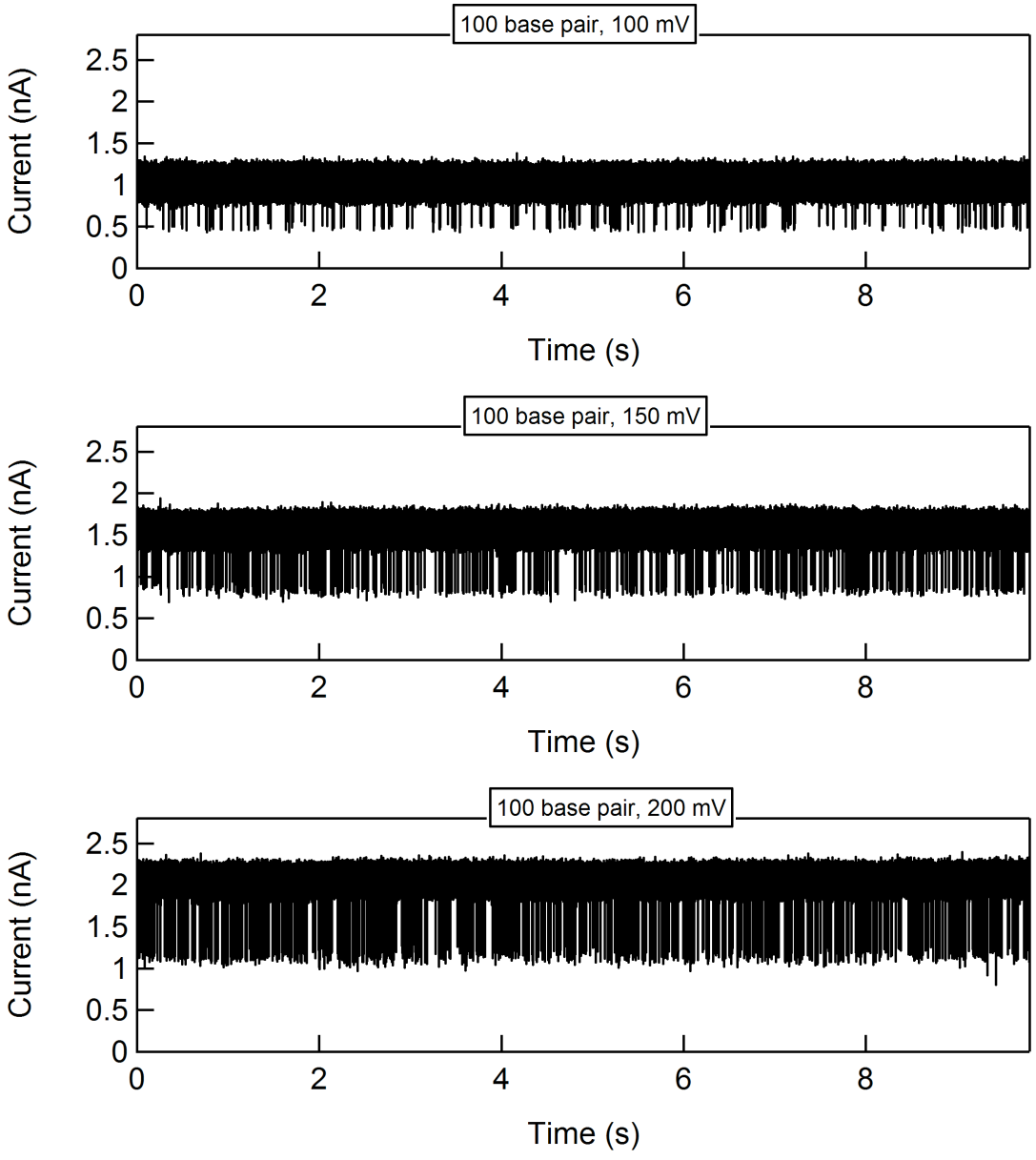

Figure S9. Unprocessed traces of dsDNA in a 3.6 nm HfO_2 pore at 100 mV, 150 mV, and 200 mV, demonstrating very uniform translocations.

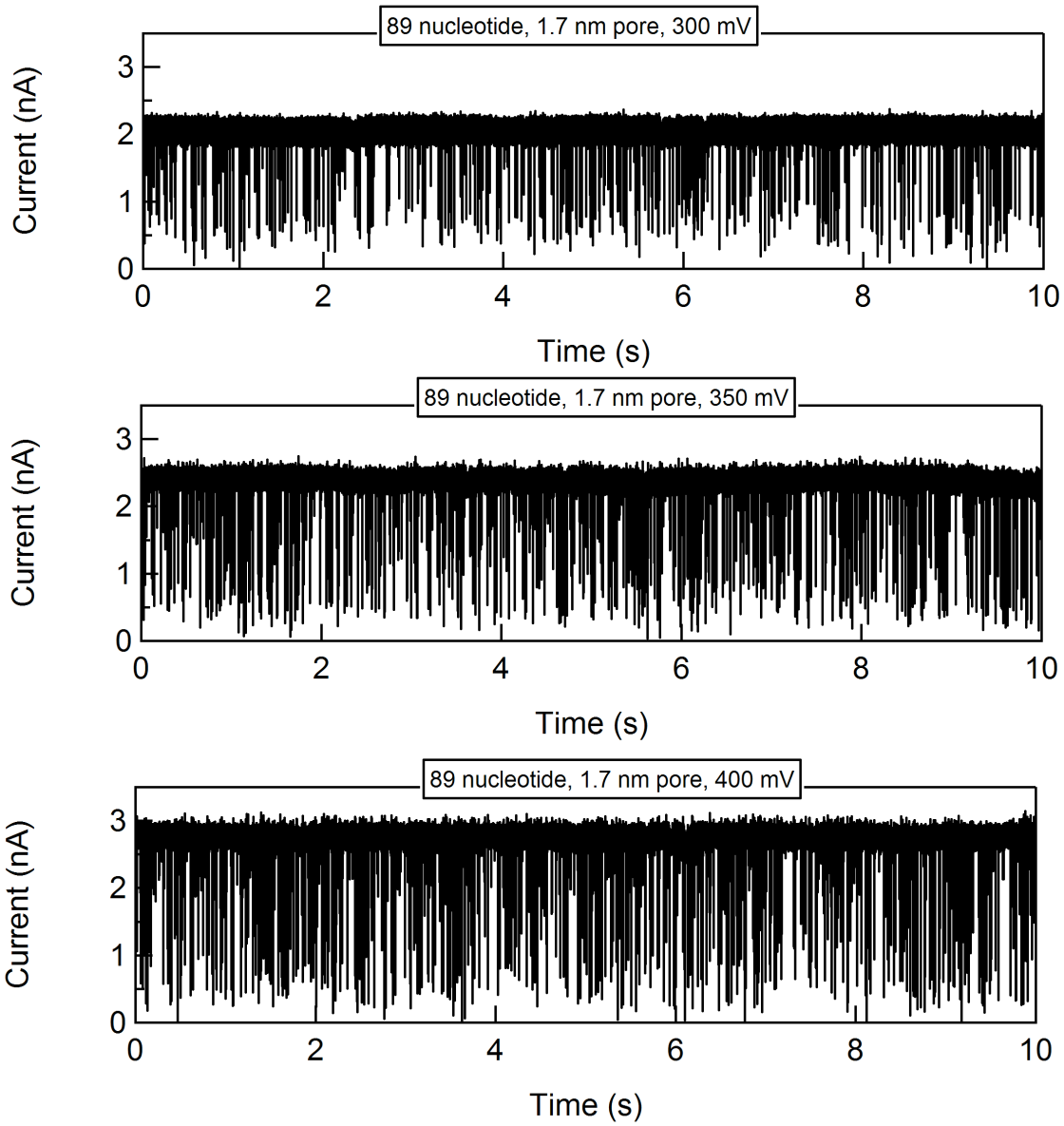

Figure S10. Unprocessed traces of ssDNA in a 1.7 nm HfO_2 pore at 300 mV, 350 mV, and 400 mV.

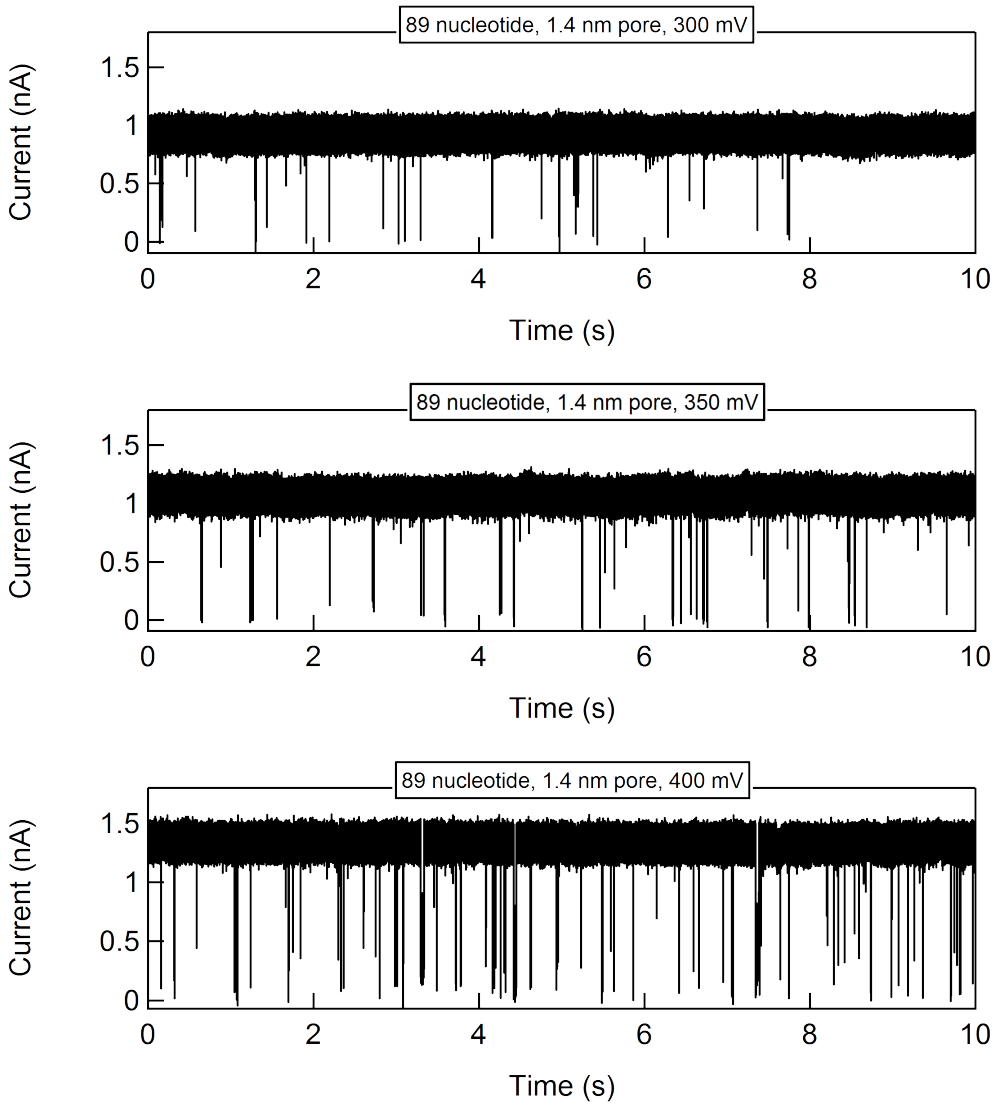

Figure S11. Unprocessed traces of ssDNA in a 1.4 nm HfO_2 pore at 300 mV, 350 mV, and 400 mV.

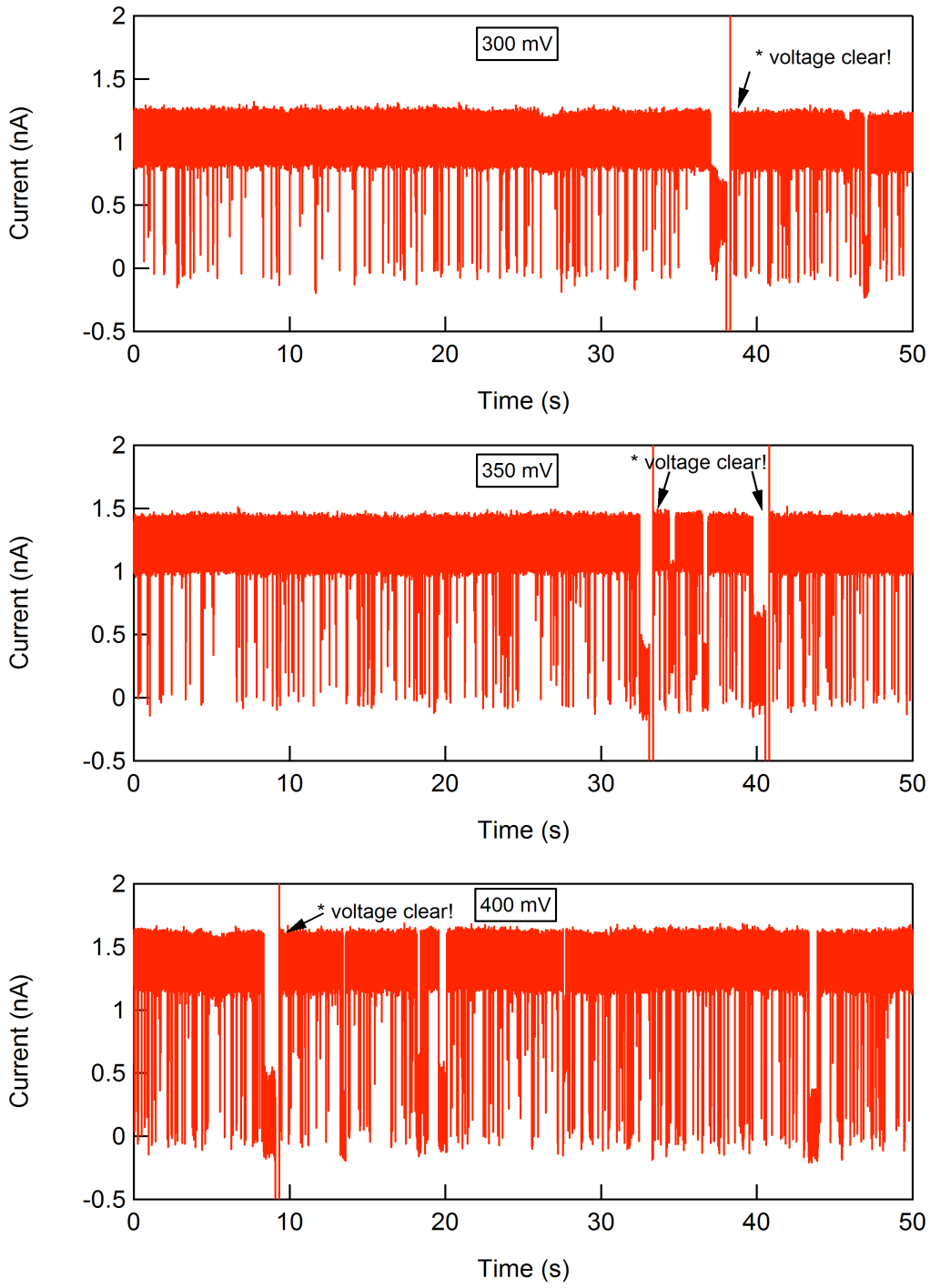

Figure S12. Representative 50-second unprocessed traces of ssDNA in a 1.4 nm HfO_2 pore at 300 mV, 350 mV, and 400 mV, showing high pore stability. Identified voltage clears are periods where the pore conductance dips below a certain threshold for a predetermined period of time (> 1 sec), where a negative voltage pulse was applied to clear the pore.

References:

1. Kim, M. J.; Wanunu, M.; Bell, D. C.; Meller, A., Rapid fabrication of uniformly sized nanopores and nanopore arrays for parallel DNA analysis, *Adv Mater* **2006,** *18* (23), 3149-3153.
2. Wanunu, M.; Morrison, W.; Rabin, Y.; Grosberg, A. Y.; Meller, A., Rapid electronic detection of probe-specific microRNAs using thin nanopore sensors, *Nat Nanotechnol* **2010,** *5* (11), 807-814.
3. Kowalczyk, S. W.; Grosberg, A. Y.; Rabin, Y.; Dekker, C., Modeling the conductance and DNA blockade of solid-state nanopores, *Nanotechnology* **2011,** *22*, 315101.
4. Wanunu, M.; Sutin, J.; McNally, B.; Chow, A.; Meller, A., DNA Translocation Governed by Interactions with Solid-State Nanopores, *Biophys J* **2008,** *95* (10), 4716-4725.
5. Meller, A.; Branton, D., Single molecule measurements of DNA transport through a nanopore, *Electrophoresis* **2002,** *23* (16), 2583-2591.